島根大学地球資源環境学研究報告　32, 13 ～22 ページ（2013 年 12 月）
Geoscience Rept. Shimane Univ., 32, p.13～22（2013）

Article

High-Mg garnets in kyanite garnet amphibolite from the Tonaru metagabbro mass in the Sambagawa metamorphic belt, Besshi district, central Shikoku, Japan

Hiroaki Matsuura*, Akira Takasu* and Md. Fazle Kabir*

Abstract

The Tonaru mass occurs as a large lenticular body in the highest-grade portions of the Sambagawa schists in the Besshi district. The mass consists of diopside amphibolite and garnet epidote amphibolite accompanied by small amounts of eclogite. Kyanite garnet amphibolites from the western parts of the Tonaru metagabbro mass are composed of amphibole (calcic-amphibole; magnesiohornblende, tschermakite), zoisite, kyanite, garnet, phengite, paragonite, margarite, chlorite, quartz and pyrite, and show banded structure consisting of alternating amphibole and zoisite-rich layers. Porphyroblastic garnets reach up to 8 cm in diameter, and show a prograde growth zoning, with X_{Prp} (0.40-0.52) increasing from core to rim. Magnesium contents are highest in the outermost rim (MgO 13.82 wt%), suggests the rims of the garnets record the peak metamorphic stage. Some microveins occur throughout the garnet. These microveins are filled by Fe-rich garnet, occasionally accompanied by zoisite. Micro-veins in the same garnet have an almandine-rich (X_{Alm} 0.45-0.50, X_{Prp} 0.25-0.34) composition. The metamorphic evolution of the kyanite garnet amphibolite from the western part of the Tonaru metagabbro mass is probably divided into two metamorphic events. The porphyroblastic high-Mg garnet represents prograde metamorphism from the epidote-blueschist facies that reached into the eclogite facies at the peak metamorphism. Fe-rich garnets developed in the microveins commonly coexist with fracture-filling minerals (kyanite, zoisite, magnesio-hornblende, tschermakite and chlorite) that are evidence of a second high-*P* metamorphic event. This second metamorphic event probably correlates with the prograde Sambagawa metamorphism of the oligoclase-biotite zone.

Key words: Sambagawa (Sanbagawa) metamorphic belt, Tonaru metagabbro mass, high-Mg garnet, kyanite, eclogite

Introduction

Garnets in metamorphic rocks are often chemically zoned, and provide one of the most important records of the pressure-temperature (*P-T*) history of metamorphism. The chemical zoning of garnets in the Sambagawa metamorphic belt usually shows a normal bell-shaped MnO profile, with decreasing MnO content from core to rim. This bell-shaped profile is considered to reflect the prograde change of *P-T* conditions during the growth of the garnet (e.g. Takasu, 1984; Sakai *et al.*, 1985; Banno *et al.*, 1986). However, other types of garnet zoning have also been reported from the Sambagawa metamorphic belt in central Shikoku, including reverse zoning (e.g. Itaya, 1978; Takasu, 1979, 1984), resorption-overgrowth (e.g. Takasu, 1986; Takasu and Fujita, 1994), and sector zoning (e.g. Kitamura *et al.*, 1993; Takasu and Kondo, 1993; Shirahata and Hirajima, 1995). In addition to these types, high-Mg zoning also occurs in garnet in the high-grade part of the Sambagawa belt in central Shikoku (e.g. Nomizo, 1992; Takasu and Kondo, 1993; Takasu and Fujita, 1994; Kabir and Takasu, 2011).

The Sambagawa metamorphic belt of southwest Japan is one of the best-studied examples of subduction-type high-pressure metamorphic belts worldwide. The Sambagawa belt extends for about 800 km throughout southwest Japan, stretching from Saganoseki Peninsula in Kyushu, through to the Kanto Mountains in the northeast (Fig. 1). Metamorphic grades range from the pumpellyite-actinolite facies through the blueschist/greenschist facies transition, to the epidote-amphibolite facies, and to the eclogite facies (e.g. Banno, 1964; Higashino, 1990; Enami *et al.*, 1994). Most parts of the Sambagawa belt underwent high-*P/T* metamorphism during the Cretaceous period (Itaya and Takasugi, 1988; Takasu and Dallmeyer, 1990; Wallis *et al.*, 2009).

The Sambagawa belt in central Shikoku consists of the Oboke nappe complex and the structurally overlying Besshi nappe complex. The Oboke nappe complex consists of low-grade psammitic and pelitic schists with minor basic, siliceous and conglomeratic schists, whereas the Besshi nappe complex is dominated by pelitic schists, intercalated basic schists, and minor amounts of siliceous and calcareous schists. In the Besshi district the metamorphism is divided into four zones based on index minerals in the pelitic schists, namely the chlorite, garnet, albite-biotite, and oligoclase-biotite zones (Fig. 1; Enami, 1983; Higashino, 1990; Enami *et al.*, 1994). The higher-grade albite-biotite and oligoclase-biotite zones are equivalent to epidote-amphibolite facies metamorphism.

Several eclogite-bearing bodies occur throughout the albite-biotite and the oligoclase-biotite zones in the high-grade portions of the metamorphic sequence in the Besshi district, such as the Higashi-akaishi and Nikubuchi peridotite bodies, the Western Iratsu, Quartz Eclogite, Seba eclogitic basic schists, and the Sebadani, Eastern Iratsu and Tonaru metagabbro masses (e.g. Yokoyama, 1980; Takasu, 1984; Kunugiza *et al.*, 1986; Takasu, 1989; Aoya, 2001; Kugimiya

*Department of Geoscience, Graduate School of Science and Engineering, Shimane University, 1060 Nishikawatsu, Matsue 690-8504, Japan

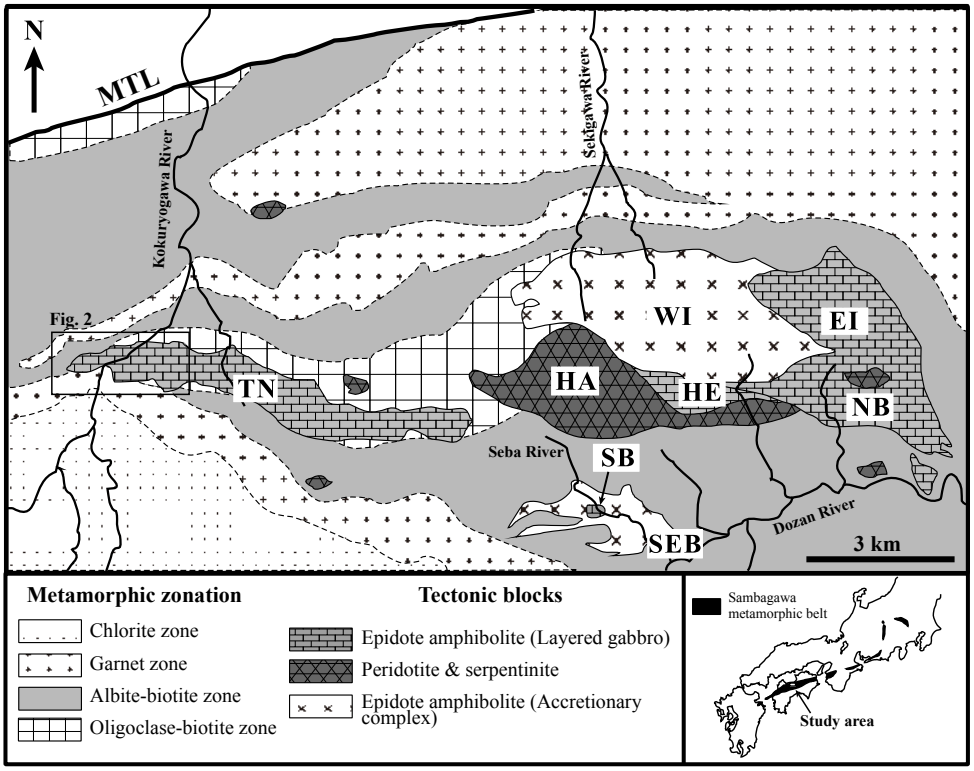

Fig. 1. Geological and metamorphic zonation map of the Sambagawa metamorphic belt in the Besshi district, central Shikoku, Japan (compiled from Takasu and Makino, 1980; Takasu, 1989; Higashino, 1990; Kugimiya and Takasu, 2002; Sakurai and Takasu, 2009; Kabir and Takasu, 2010a). SB, Sebadani metagabbro mass; SEB, Seba basic schists; TN, Tonaru metagabbro mass; WI, Western Iratsu mass; EI, Eastern Iratsu mass; HA, Higashi-akaishi peridotite mass; HE, Hornblende eclogite mass; NB, Nikubuchi peridotite mass; MTL, Median Tectonic Line. Location for Figure 2 is also shown.

and Takasu, 2002; Ota *et al.*, 2004; Miyagi and Takasu, 2005; Kabir and Takasu, 2010a, b; Endo and Tsuboi, 2013) (Fig. 1).

The Tonaru metagabbro mass (~6.5 km × 1 km) is one of the eclogite-bearing bodies located in the central part of the Besshi district, and lies within the highest grade oligoclase-biotite zone of the Sambagawa sequence (Higashino, 1990) (Fig. 1). Compositional banding that reflects the original layered structure is widely developed in the mass, with schistosity defined by epidote-amphibolite facies minerals. The Tonaru metagabbro mass is considered to have been derived from a layered gabbro (Banno *et al.*, 1976; Kunugiza *et al.*, 1986; Takasu, 1989). The Tonaru mass occurs as a large lenticular body consisting of diopside amphibolite (T-I type amphibolite) with small amounts of associated serpentinite, and garnet epidote amphibolite (T-II type amphibolite) accompanied by small amounts of eclogite (Moriyama, 1990) (Fig. 2). Kunugiza (1984) suggested that serpentinites within the diopside amphibolites were originally peridotites that were serpentinized, followed by subsequent prograde metamorphism. Takasu *et al.* (1994) suggested that the eclogite-bearing garnet epidote amphibolites underwent eclogite facies metamorphism before being retrograded into the epidote-amphibolite facies.

Miyagi and Takasu (2005) reported detailed petrology and a metamorphic history of the Tonaru metagabbro mass. They suggested that the Tonaru metagabbro mass underwent three metamorphic events. A high-*T* amphibolite facies (i) precursor metamorphic event that occurred before the prograde eclogite facies metamorphism is characterized by pargasite-taramite inclusions in the low-Ca inner cores of porphyroblastic garnets and Mg-rich relict cores of garnet (MgO ~ 8 wt%). The first high-*P* metamorphic event of the eclogite facies (ii) led to prograde metamorphism from the epidote-blueschist facies (300-450°C and 7-11 kbar) to the eclogite facies (700-730°C and ≥ 15 kbar), and subsequent retrogression into epidote-amphibolite facies. The mass subsequently underwent another prograde metamorphism (iii) together with the surrounding Sambagawa schists, reaching oligoclase-biotite zone metamorphic conditions.

In this study we describe the texture, modes of occurrence and the chemical compositions of high-Mg garnets found in kyanite garnet amphibolite from the western part of the Tonaru metagabbro mass. The mineral abbreviations used in the text, tables, and figures follow Whitney and Evans (2010).

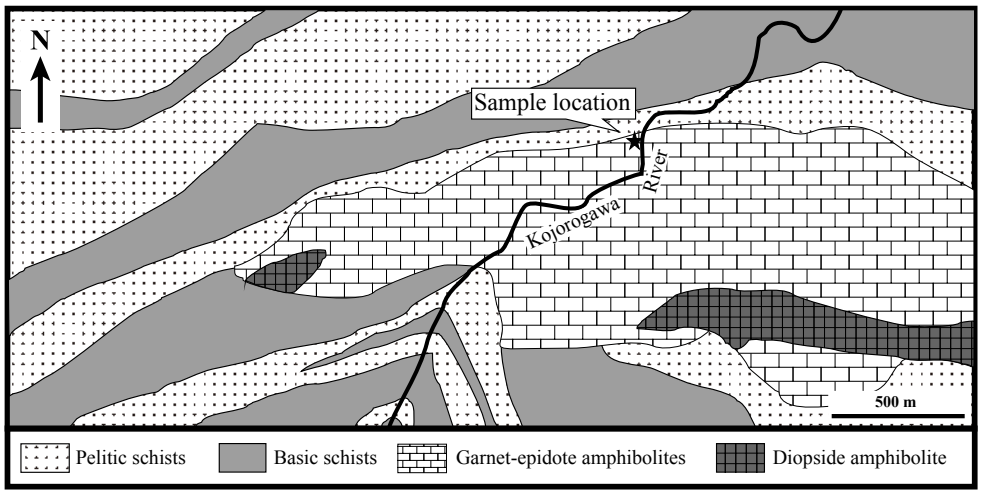

Fig. 2. Lithological map of the Tonaru metagabbro mass in the Kojorogawa River (after Miyagi and Takasu, 2005), with sample location.

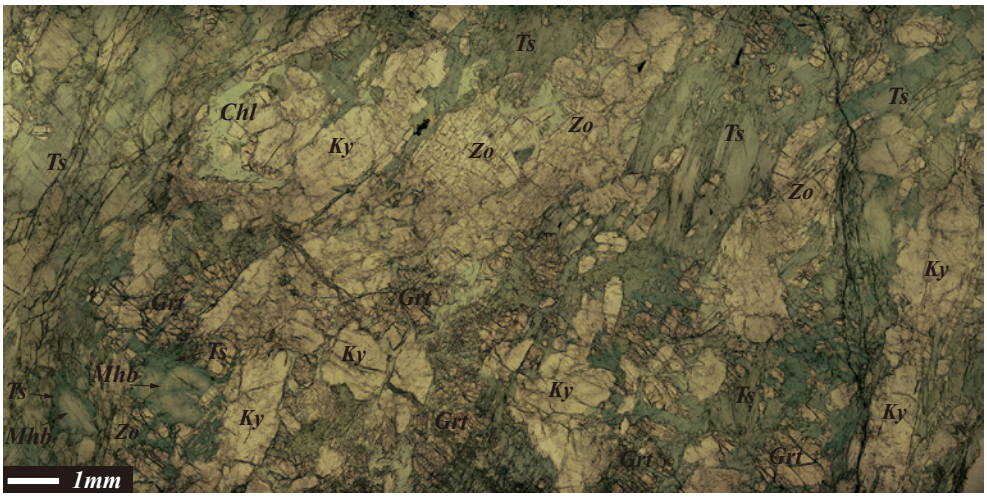

Fig. 3. Photomicrograph of the kyanite garnet amphibolite from the Tonaru metagabbro mass (sample MT18) showing the schistosity-forming matrix minerals kyanite, garnet, zoisite and amphibole.

Petrography of the garnet amphibolite

Several garnet amphibolite samples were collected along the Kojorogawa River from the western part of the Tonaru metagabbro mass. Two types of garnet amphibolite have been distinguished: kyanite-bearing (kyanite garnet amphibolite) and kyanite-free garnet amphibolites. Two representative samples (MT18 and MT13) were selected for detailed petrography.

Kyanite garnet amphibolite (MT18):

Kyanite garnet amphibolites from the western parts of the Tonaru metagabbro mass are composed mainly of amphibole (calcic-amphibole; magnesiohornblende, tschermakite), zoisite, kyanite and garnet. Minor phengite occurs, along with accessory amounts of paragonite, margarite, chlorite, quartz, corundum and pyrite (Fig. 3). Preferred orientation of amphibole, zoisite and kyanite defines schistosity and mineral lineation. Banded structure consists of alternating amphibole and zoisite-rich layers.

Garnet occurs as anhedral porphyroblasts up to 8 cm across, and it is typically zoned, with pale orange inclusion-rich core and colorless inclusion-poor rim (Fig. 4). Garnet contains inclusions of zoisite and few phengite (Si 6.42-6.65 pfu), paragonite and quartz. Most of the garnets are severely fractured and the fractures are filled by the aggregates of kyanite, chlorite, zoisite and amphibole (magnesiohornblende, tschermakite). Some microveins occur throughout the garnets. These microveins are filled by Fe-rich garnet, occasionally accompanied by zoisite (Fig. 4).

Prismatic amphiboles up to 1.5 mm across occur in the matrix. Most of them are zoned, with magnesiohornblende cores and tschermakite rims. Amphiboles filling the fractures of the garnets (magnesiohornblende, tschermakite) are anhedral in shape, and also display the same compositional

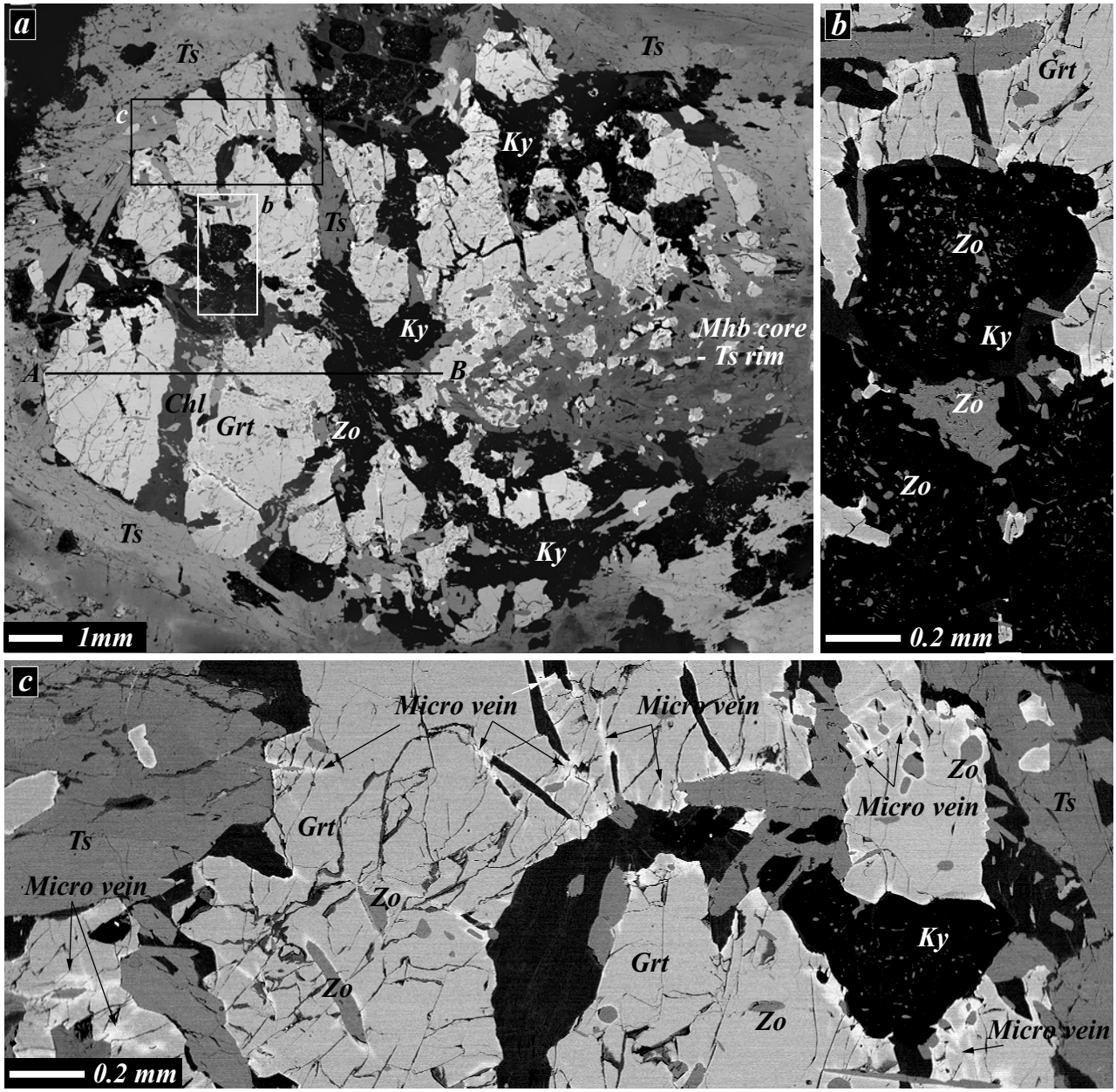

Fig. 4. Backscattered electron (BSE) image of garnet in kyanite garnet amphibolite from the Tonaru metagabbro mass (sample MT18). (a) The garnet contains fine-grained inclusions of zoisite. Fractures in the garnets are filled by aggregates of kyanite, chlorite, zoisite and amphibole (magnesiohornblende, tschermakite). Line (A-B) shows the location of the garnet compositional profile shown in Fig. 5. (b) Kyanite in the garnet fracture contains zoisite inclusions. (c) Garnet containing microveins. Zoisite is occasionally included within the microveins.

zoning as the matrix amphiboles.

Zoisite has two modes of occurrence. Schistosity-forming zoisite (X_{Ps} 0.03-0.06) is found as subhedral prismatic grains up to 0.7 mm in length. Zoisites occurring as inclusions in garnet (X_{Ps} 0.04-0.07) and in kyanite (X_{Ps} 0.04-0.05) are smaller, with grain size of up to 0.4 mm across.

Two modes of occurrence of kyanite were recognized. Prismatic crystals in the matrix are up to 2 cm in length, whereas irregularly shaped kyanite grains up to 1 mm across occur within fractures in garnet. Some kyanites in the matrix are replaced by symplectites consisting of paragonite, margarite, chlorite and corundum. A small amount of phengite (Si 6.42-6.65 pfu) occurs as inclusions in garnet. This phengite is mostly rimmed by paragonite.

Kyanite-free garnet amphibolite (MT13):

Kyanite-free garnet amphibolite (Garnet epidote-amphibolite as described by Miyagi and Takasu, 2005) is composed mainly of amphiboles (magnesiohornblende, tschermakite, pargasite), epidote and garnet. Minor amounts of plagioclase (An 1-18), muscovite (Si 6.04-6.13 pfu), phengite (Si 6.27-6.82 pfu), paragonite, chlorite and quartz, and accessory

rutile occur as constituent minerals. Preferred orientation of amphibole, epidote, phengite and paragonite defines a schistosity and a mineral lineation.

Garnet occurs as subhedral porphyroblasts up to 1.5 cm across. These contain inclusions of quartz, rutile, epidote, paragonite, phengite (Si 6.27-6.82 pfu) and amphibole-quartz symplectite.

Amphibole has two modes of occurrence, being found as fine-grained amphibole and schistosity-forming amphibole. Fine-grained amphibole (tschermakite, pargasite) is a constituent of symplectitic aggregates of amphibole and quartz occurring as inclusions in garnets. The symplectite inclusions are connected to the exteriors of the garnets. Schistosity-forming amphibole grains reach 1.0 mm in length, and are commonly zoned from magnesiohornblende cores to tschermakite and pargasite rims.

Phengite (Si 6.27-6.82 pfu) occurs as inclusions up to 1 mm in length within garnet. Muscovite grains (Si 6.04-6.13 pfu) occurring in the matrix reach 3 mm in width. Paragonite occurring as inclusions in the garnet and in the matrix is coarser (5 mm) than the other micas. Paragonite is interlayered with phengite and muscovite.

Epidote has three modes of occurrence: as inclusions in garnet, in the matrix, and in epidote-quartz symplectite surrounding amphibole in the matrix. Epidote inclusions (X_{Ps} 0.19-0.21) in the garnets reach 0.3 mm in diameter. Schistosity-forming epidote is up to 0.8 mm across, and is zoned (X_{Ps} 0.15-0.18 cores and 0.19-0.21 rims). Epidote (X_{Ps} 0.23-0.30) occurring as a constituent of epidote-quartz symplectite surrounding amphibole is fine-grained (0.5 mm).

Chemical compositions of the high-Mg garnets

Chemical compositions and compositional zoning of the garnets in the kyanite garnet amphibolite from the western parts of the Tonaru metagabbro mass were investigated in Shimane University, using JEOL JXA 8800M and JXA 8530F electron microprobe analyzers. Analytical conditions used for quantitative analysis were 15 kV accelerating voltage, 20 nA specimen current, and 5 μm beam diameter. Correction procedure was carried out as described by Bence and Albee (1968). Ferric iron contents in garnet were estimated using charge balance $Fe^{3+} = 8\text{-}2Si\text{-}2Ti\text{-}Al$ (O = 12). Contents of Na (< 0.01 pfu), K (< 0.01 pfu) and Cr (< 0.01 pfu) were negligible.

The porphyroblastic garnets have pyrope (X_{Prp} 0.32-0.52) and almandine-rich composition (X_{Alm} 0.30-0.47), with considerable amounts of the grossular (X_{Grs} 0.08-0.20) and small amounts of spessartine (X_{Sps} 0.01-0.03) components. The garnets within microveins are almandine-rich (X_{Alm} 0.43-0.53), and they are slightly richer in spessartine (X_{Sps} 0.02-0.07) and poorer in pyrope (X_{Prp} 0.24-0.39) than the host garnets. Grossular content (X_{Grs} 0.11-0.19) does not vary significantly, compared with the Mg-rich host garnet.

The garnets show prograde zoning, with X_{Prp} increasing gently from the inner core to the outer core (0.40-0.45) and sharply increasing towards the rim (0.45-0.52) (Table 1; Figs. 5, 6). X_{Alm} also shows zoning, decreasing gently from the inner core to the outer core (0.40-0.36) and decreasing sharply towards the rim (0.36-0.30). X_{Sps} decreases gently from core to rim (X_{Sps} 0.03-0.01). X_{Grs} is almost uniform or decreases slightly from core to rim (0.12-0.08). X_{Mg} [$Mg / (Mg + Fe^{2+})$] increases from the inner core to the outer core (0.49-0.54), as well as from outer core to the rim (0.55-0.61). Micro-veins in the same garnet have a composition of almandine (X_{Alm} 0.45-0.50), and pyrope (X_{Prp} 0.25-0.34) with minor spessartine (X_{Sps} 0.04-0.07) and grossular (X_{Grs} 0.11-0.13) components (Figs. 5, 6). X_{Mg} shows slight variation, from 0.33 to 0.42.

Discussion and Conclusions

High-Mg garnets in the kyanite garnet amphibolite from the Tonaru metagabbro mass provide important information on the Sambagawa metamorphism. The garnets show a prograde zoning, and display highest Mg content in the outermost rim (MgO 13.82 wt%), suggesting the rim of the garnet records evidence of the peak metamorphic stage. Banno (1966) also reported Mg-rich garnet (MgO 9.9 wt%) from a quartz-kyanite-zoisite-hornblende-garnet rock that was collected along the Kojorogawa River, at the northern border of the Tonaru mass. Miyagi and Takasu (2005) reported a porphyroblastic garnet containing a relict Mg-rich resorbed core (MgO 8 wt%) overgrown by Mg-poor garnet in kyanite-free garnet epidote amphibolites in the central part of the Tonaru mass. They suggested that the core of the garnet was evidence of the precursor metamorphic stage before the high-*P* eclogite facies metamorphism, and that the Mg-poor rim represented eclogite facies metamorphism.

Miyagi and Takasu (2005) reported three modes of occurrence of garnet in the garnet epidote-amphibolite, i.e. porphyroblastic garnet, fine-grained garnet, and high-Mg

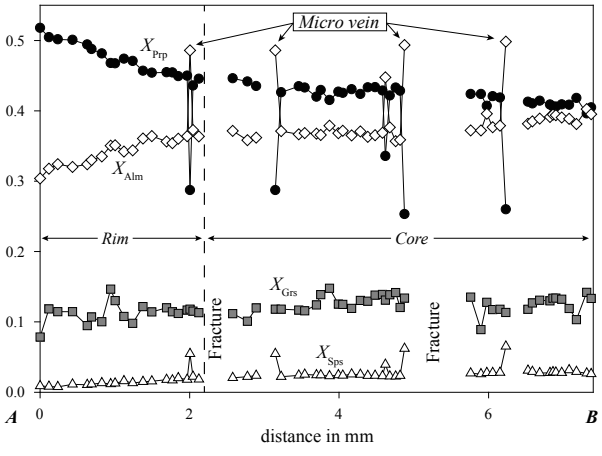

Fig. 5. Compositional profile of a zoned garnet from kyanite garnet amphibolites.

Figure 6 (Matsuura et al.)

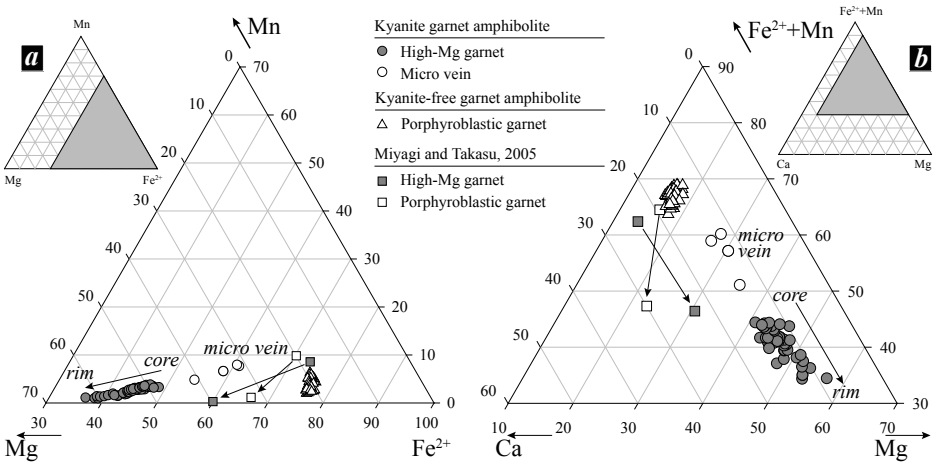

Fig. 6. (a-b) Composition of garnet from the kyanite garnet amphibolite and kyanite-free garnet amphibolites (this study) in terms of Fe^{2+}, Mn, Mg and Ca. Garnet compositions from the garnet epidote amphibolite of Miyagi and Takasu (2005) are also shown.

fragmental porphyroblastic garnet. Porphyroblastic garnets are almandine-rich, and X_{Mg} increases from core to rim (0.22-0.33) (Fig. 6). The chemical compositions of fine-grained garnets are fairly homogeneous, and X_{Mg} slightly increases toward the rim (0.23-0.30). The compositions are similar to those of the rims of the porphyroblastic garnets. Mg-rich fragmented porphyroblastic garnets in the garnet epidote amphibolites show Mg-rich composition, and zoning with resorbed cores (X_{Mg} 0.40) and Mg-poor and Mn-rich rims (X_{Mg} 0.20).

The garnet in the kyanite-free garnet amphibolite in the present study is almandine-rich, and X_{Mg} slightly increases form core to rim (0.20-0.22) (Fig. 6). Garnet in the kyanite-free garnet amphibolite shows similar X_{Mg} (within the range), whereas that in the kyanite garnet amphibolite has significantly higher X_{Mg} than the high-Mg garnet of Miyagi and Takasu (2005). Amphibole in the kyanite garnet amphibolite has higher X_{Mg} (0.85-1.00) than those in the kyanite-free garnet amphibolite (0.62-0.74) and garnet epidote amphibolite (0.33-0.78) of Miyagi and Takasu (2005). Phengite and paragonite in the kyanite garnet amphibolite also show higher X_{Mg} (Ph 0.72-0.77, Pg 0.50-0.67) than those from the kyanite-free garnet amphibolite (Ph 0.41-0.54, Pg 0.40-0.50) and garnet epidote amphibolite (Ph 0.60-0.67, Pg 0.12-0.33) of Miyagi and Takasu (2005).

Kyanite garnet amphibolites collected from the western parts of the Tonaru metagabbro mass in the present study contain porphyroblastic high-Mg garnet with microveins filled by Fe-rich garnet, suggesting two stages of garnet growth. The texture of the porphyroblastic garnet is similar to that of the Mg-poor rims of the Miyagi and Takasu (2005) garnet, although Mg content is distinctly higher. X_{Mg} contents of garnet, amphibole and white micas in the kyanite garnet amphibolite are greater than those in kyanite-free garnet amphibolite and garnet epidote amphibolite (Miyagi and Takasu, 2005).

Based on petrography and the chemical composition of the constituent minerals, the metamorphic evolution of the kyanite garnet amphibolite from the western part of the Tonaru metagabbro mass can be divided into two metamorphic events. These are a first high-pressure metamorphic event (i) represented by high-Mg garnet and inclusions in the garnets (zoisite, phengite, paragonite and quartz), and a second high-pressure metamorphic event (ii) recorded by the mineral assemblage of kyanite, zoisite, amphibole (magnesiohornblende, tschermakite) and chlorite developed in the garnet fractures, as well as in the matrix. The high-Mg garnets in the kyanite garnet amphibolite formed in the prograde metamorphism of high-*P* metamorphic event; during the retrograde metamorphism the porphyroblastic garnets were strongly fractured. Miyagi and Takasu (2005) reported a *P-T* path of eclogite and garnet epidote amphibolite metamorphism. The prograde path passes through the epidote-blueschist facies to the eclogite facies peak at 700-730°C and ≥ 15 kbar, followed by retrograde metamorphism into the epidote-amphibolite facies. The porphyroblastic garnet in the present study probably follow a similar prograde, peak and retrograde *P-T* path of Tonaru eclogite and garnet epidote amphibolite. Fe-rich garnets developed, as the microveins probably coexisted with the fracture-filling minerals of kyanite, zoisite, amphibole (magnesiohornblende, tschermakite) and chlorite. These provide evidence of the second high-*P* metamorphic event. This metamorphic event was probably similar to that of the prograde Sambagawa metamorphism of the oligoclase-biotite zone, as reported by Miyagi and Takasu (2005).

Acknowledgements

We thank the members of the Metamorphic Geology seminar of Shimane University for discussion and helpful

suggestions, and B. P. Roser for critical reading and comments on the manuscript. Thanks are also due to Yasunori Kondo for his support during fieldwork. This study was partly supported by JSPS KAKENHI Grant (No. 24340123) to A.T.

References

Aoya, M., 2001, *P-T-D* path of eclogite from the Sambagawa belt deduced from combination of petrological and microstructural analyses. *Journal of Petrology*, **42**, 1225-1248.

Banno, S., 1964, Petrological studies of the Sanbagawa crystalline schists in the Bessi-Ino district, central Shikoku, Japan. *Journal of the Faculty of Science, Tokyo University, Section II*, **15**, 203-319.

Banno, S., 1966, Eclogite and eclogite facies. *Japanese Journal of Geology and Geography*, **37**, 105-122.

Banno, S., Sakai, C. and Higashino, T., 1986, Pressure-temperature trajectory of the Sanbagawa metamorphism deduced from garnet zoning. *Lithos*, **19**, 51-63.

Banno, S., Yokohama, K., Enami, M., Iwata, O., Nakamura, K. and Kasashima, S., 1976, Petrography of the peridotite-metagabbro complex in the vicinity of Mt. Higashi-akaishi, Central Shikoku. Part I. Megascopic textures of the Iratsu and Tonaru epidote amphibolite masses. *The Science Reports of Kanazawa University*, **21**, 139-159.

Bence, A. E. and Albee, A. L., 1968, Empirical correction factors for the electron microanalysis of silicates and oxides. *Journal of Geology*, **76**, 382-403.

Enami, M., 1983, Petrology of pelitic schists in the oligoclase-biotite zone of the Sanbagawa metamorphic terrain, Japan: phase equilibria in the highest grade zone of a high-pressure intermediate type of metamorphic belt. *Journal of Metamorphic Geology*, **1**, 141-161.

Enami, M., Wallis, S. R. and Banno, Y., 1994, Paragenesis of sodic pyroxene-bearing quartz schists: implications for the *P-T* history of the Sanbagawa belt. *Contributions to Mineralogy and Petrology*, **116**, 182-198.

Endo, S. and Tsuboi, M., 2013, Petrogenesis and implications of jadeite-bearing kyanite eclogite from the Sanbagawa belt (SW Japan). *Journal of Metamorphic Geology*, **31**, 647-661.

Higashino, T., 1990, The higher grade metamorphic zonation of the Sambagawa metamorphic belt in central Shikoku, Japan. *Journal of Metamorphic Geology*, **8**, 413-423.

Itaya, T., 1978, Reverse-zoned garnet in Sanbagawa pelitic schists in central Shikoku, Japan. *The Journal of the Japanese Association of Mineralogists, Petrologists and Economic Geologists*, **73**, 393-396.

Itaya, T. and Takasugi, H., 1988, Muscovite K-Ar ages of the Sanbagawa schists, Japan and argon depletion during cooling and deformation. *Contributions to Mineralogy and Petrology*, **100**, 281-290.

Kabir, M. F. and Takasu, A., 2010a, Evidence for multiple burial-partial exhumation cycles from the Onodani eclogites in the Sambagawa metamorphic belt, central Shikoku, Japan. *Journal of Metamorphic Geology*, **28**, 873-893.

Kabir, M. F. and Takasu, A., 2010b, Glaucophanic amphibole in the Seba eclogitic basic schists, Sambagawa metamorphic belt, central Shikoku, Japan: implications for timing of juxtaposition of the eclogite body with the non-eclogite Sambagawa schists. *Earth Sciences*, **64**, 183-192.

Kabir, M. F. and Takasu, A., 2011, High-Mg garnets from pelitic schists adjacent to the Sebadani eclogitic metagabbro mass, Sambagawa metamorphic belt, central Shikoku, Japan. *Journal of Mineralogical and Petrological Sciences*, **106**, 332-337.

Kitamura, M., Wallis, S. R. and Hirajima, T., 1993, Sector zoning and surface roughening of garnet in the Sambagawa metamorphic rocks. In: *6th Topical Meetting on Crystal Growth Mechanism*, pp. 215-220.

Kugimiya, Y. and Takasu, A., 2002, Geology of the Western Iratsu mass within the tectonic melange zone in the Sambagawa metamorphic belt, Besshi district, central Shikoku, Japan. *Journal of the Geological Society of Japan*, **108**, 644-662.

Kunugiza, K., 1984, Metamorphism and origin of ultramafic bodies of the Sanbagawa Metamorphic Belt in central Shikoku. *Journal of the Japanese Association for Mineralogists, Petrologists and Economic Geologists*, **79**, 20-32.

Kunugiza, K., Takasu, A. and Banno, S., 1986, The origin and metamorphic history of the ultramafic and metagabbro bodies in the Sanbagawa Metamorphic Belt. *Geological Society of America Memoir*, **164**, 375-386.

Miyagi, Y. and Takasu, A., 2005, Prograde eclogites from the Tonaru epidote amphibolite mass in the Sambagawa Metamorphic Belt, central Shikoku, southwest Japan. *Island Arc*, **14**, 215-235.

Moriyama, H., 1990, Two metamorphic paths in the Tonaru epidote amphibolite mass within the Sambagawa belt, Besshi district, central Shikoku. *Geoscience Reports of Shimane University, Japan*, **9**, 49-54.

Nomizo, A., 1992, Three types of garnet in a Sambagawa pelitic schist near the Sebadani eclogite mass, central Shikoku, Japan. *Journal of Geological Society of Japan*, **98**, 49-52.

Ota, T., Terabayashi, M. and Katayama, I., 2004, Thermobaric structure and metamorphic evolution of the Iratsu eclogite body in the Sanbagawa belt, central Shikoku, Japan. *Lithos*, **73**, 95-126.

Sakai, C., Banno, S., Toriumi, M. and Higashino, T., 1985, Growth history of garnet in pelitic schists of the Sanbagawa metamorphic terrain in central Shikoku. *Lithos*, **18**, 81-95.

Sakurai, T. and Takasu, A., 2009, Geology and metamorphism of the Gazo mass (eclogite-bearing tectonic block) in the Sambagawa metamorphic belt, Besshi district, central Shikoku, Japan. *Journal of Geological Society of Japan*, **115**, 101-121.

Shirahata, K. and Hirajima, T., 1995, Chemically sector-zoned garnet in Sanbagawa schists; its mode of occurrence and growth timing. *Journal of Mineralogy Petrology and Economic Geology*, **90**, 69-79.

Takasu, A., 1979, Basic intrusive rocks and metamorphism of the Sambagawa belt in the Besshi district, Shikoku. *Magma*, **56**, 8-14.

Takasu, A., 1984, Prograde and retrograde eclogites in the Sambagawa metamorphic belt, Besshi district, Japan. *Journal of Petrology*, **25**, 619-643.

Takasu, A., 1986, Resorption-overgrowth of garnet from the Sambagawa pelitic schists in the contact aureole of the Sebadani metagabbro mass, Shikoku, Japan. *Journal of the Geological Society of Japan*, **92**, 781-792.

Takasu, A., 1989, *P-T* histories of peridotite and amphibolite tectonic blocks in the Sanbagawa metamorphic belt, Japan. In: *Evolution of Metamorphic Belts* (eds Daly, J. S., Cliff, R. A. & Yardley, B. W. D.), pp. 533-538, Blackwell Scientific Publications, Oxford, Geological Society, London, Special Publications.

Takasu, A. and Dallmeyer, R. D., 1990, $^{40}Ar/^{39}Ar$ mineral age constraints for the tectonothermal evolution of the Sambagawa metamorphic belt, central Shikoku, Japan: a Cretaceous accretionary prism. *Tectonophysics*, **185**, 111-139.

Takasu, A. and Fujita, Y., 1994, Resorption-overgrowth garnets from the Sambagawa pelitic schists in the Besshi district, central Shikoku, Japan. *Earth Science*, **48**, 8-13.

Takasu, A. and Kondo, Y., 1993, Color map photos of the Sambagawa garnets. *Earth Science*, **47**, 1-3 (in Japanese).

Takasu, A. and Makino, K., 1980, Stratigraphy and geologic structure of the Sanbagawa metamorphic belt in the Besshi district, Shikoku, Japan (Reexamination of the recumbent fold structures). *Earth Science (Chikyu Kagaku)*, **34**, 16-26 (in Japanese with English abstract).

Takasu, A., Wallis, S. R., Banno, S. and Dallmeyer, R. D., 1994, Evolution of the Sambagawa metamorphic belt, Japan. *Lithos*, **33**, 119-133.

Wallis, S. R., Anczkiewicz, R., Endo, S., Aoya, M., Platt, J. P., Thirlwall, M. and Hirata, T., 2009, Plate movements, ductile deformation and geochronology of the Sanbagawa belt, SW Japan: tectonic significance of 89-88 Ma Lu-Hf eclogite ages. *Journal of Metamorphic Geology*, **27**, 93-105.

Whitney, D. L. and Evans, B. W., 2010, Abbreviations for names of rock-forming minerals. *American Mineralogist*, **95**, 185-187.

Yokoyama, K., 1980, Nikubuchi peridotite body in the Sanbagawa metamorphic belt; thermal history of the 'Al-pyroxene-rich suite'peridotite body in high pressure metamorphic terrain. *Contributions to Mineralogy and Petrology*, **73**, 1-13.

(Received: Nov. 20, 2013, Accepted: Dec. 5, 2013)

（要　旨）

松浦弘明・高須　晃・Kabir Md. Fazle, 2013 四国中央部別子地域三波川変成帯の東平変斑れい岩体を構成する藍晶石ざくろ石角閃岩中の高 Mg ざくろ石．島根大学地球資源環境学研究報告，32, 13-22.

東平変斑れい岩体は三波川変成帯の最も変成度の高い地域に巨大なレンズ状の岩体として産出する．岩体は少量の蛇紋岩を伴う透輝石角閃岩と少量のエクロジャイトを伴うざくろ石緑れん石角閃岩からなる．東平岩体西部に産する藍晶石ざくろ石角閃岩は角閃石（カルシウム角閃石；マグネシオホルンブレンド，チェルマク閃石），ゾイサイト，藍晶石，ざくろ石，フェンジャイト，パラゴナイト，マーガライト，緑泥石，石英，黄鉄鉱からなる．これらは角閃石に富む層とゾイサイトに富む層の互層からなる層状構造を示す．藍晶石ざくろ石角閃岩中のざくろ石斑晶変晶は直径最大 8 cm に及び粗粒である．このざくろ石は核部から縁部にかけて X_{Prp}（0.40-0.52）が増加し，累進的な累帯構造を示す．最外縁部で最も高い Mg（MgO=13.82 wt%）を示すことから，ざくろ石の縁部はピーク変成ステージを示すと考えられる．ざくろ石中には細脈が発達し，この細脈はゾイサイトを伴う Fe に富むざくろ石によって埋められている．このざくろ石中の細脈はアルマンディン成分に富み，パイロープ成分に乏しい（X_{Alm} 0.45-0.50, X_{Prp} 0.25-0.34）組成を示す．藍晶石ざくろ石角閃岩の変成作用は二回の変成イベントに分けることができる．パイロープ成分に富む粗粒なざくろ石斑晶変晶は緑れん石青色片岩相からピーク変成ステージであるエクロジャイトステージへの昇温変成作用を意味する．細脈中に発達したアルマンディン成分に富むざくろ石と共生していると考えられる割れ目を満たしている鉱物（緑泥石，マグネシオホルンブレンド～チェルマク閃石，ゾイサイト，藍晶石）は二回目の高圧変成イベントの際に形成された．この変成イベントはオリゴクレース－黒雲母帯の三波川昇温変成ステージに対比できる可能性がある．

Table 1. Representative chemical compositions of garnets from the kyanite garnet amphibolites.

Sample	MT 18																		
Analysis	1	2	3	4	5	6	7	8	9	10	11	12	13	14	15	16	17	62	18
	Rim	←	←	←	←	←	←	←	←	←	←	←	←	←	←	←	←	Vein	←
SiO_2	39.91	40.24	39.93	40.18	39.75	39.92	39.96	40.00	40.10	39.68	39.89	39.69	39.91	39.71	39.66	39.71	39.99	38.73	39.61
TiO_2	0.00	0.02	0.02	0.03	0.03	0.04	0.00	0.00	0.03	0.00	0.02	0.02	0.04	0.02	0.02	0.03	0.03	0.02	0.00
Al_2O_3	23.55	23.51	23.44	23.47	23.46	23.44	23.39	23.34	23.37	23.41	23.43	23.30	23.29	23.40	23.16	23.22	23.38	22.51	23.21
FeO*	17.60	17.00	17.18	17.18	18.00	17.92	18.36	17.49	18.11	18.24	18.94	18.63	19.11	18.62	18.79	19.05	19.13	24.23	19.44
MnO	0.42	0.38	0.36	0.53	0.50	0.54	0.62	0.55	0.60	0.75	0.62	0.69	0.74	0.84	0.80	0.95	0.85	2.49	1.04
MgO	13.82	13.61	13.38	13.48	13.16	13.05	12.87	12.53	12.56	12.60	12.59	12.15	12.15	12.10	12.08	11.96	12.06	7.46	11.57
CaO	6.28	6.37	6.19	6.28	6.34	6.36	6.33	6.32	6.32	6.21	6.41	6.20	6.18	6.33	6.45	6.30	6.27	6.21	6.24
Total	101.58	101.13	100.50	101.15	101.24	101.27	101.53	100.23	101.09	100.89	101.90	100.68	101.42	101.02	100.96	101.22	101.71	101.65	101.11
Cations on the basis of 12 oxygens																			
Si	2.92	2.95	2.95	2.95	2.93	2.94	2.94	2.97	2.96	2.94	2.93	2.95	2.95	2.94	2.94	2.94	2.95	2.95	2.94
Ti	0.00	0.00	0.00	0.00	0.00	0.00	0.00	0.00	0.00	0.00	0.00	0.00	0.00	0.00	0.00	0.00	0.00	0.00	0.00
Al	2.03	2.03	2.04	2.03	2.04	2.03	2.03	2.04	2.03	2.04	2.03	2.04	2.03	2.04	2.03	2.03	2.03	2.03	2.03
Fe^{3+}	0.94	0.97	0.98	0.98	1.00	1.01	1.03	1.05	1.06	1.04	1.06	1.09	1.11	1.08	1.08	1.10	1.11	1.13	1.11
Fe^{2+}	0.13	0.07	0.08	0.08	0.11	0.09	0.10	0.04	0.06	0.09	0.11	0.07	0.07	0.07	0.09	0.08	0.07	0.08	0.08
Mn	0.03	0.02	0.02	0.03	0.03	0.03	0.04	0.03	0.04	0.05	0.04	0.04	0.05	0.05	0.05	0.06	0.05	0.07	0.05
Mg	1.51	1.49	1.47	1.47	1.45	1.43	1.41	1.38	1.38	1.39	1.38	1.34	1.34	1.34	1.34	1.32	1.33	1.28	1.31
Ca	0.49	0.50	0.49	0.49	0.50	0.50	0.50	0.50	0.50	0.49	0.51	0.49	0.49	0.50	0.51	0.50	0.50	0.50	0.51
Total	8.05	8.03	8.03	8.03	8.06	8.03	8.05	8.01	8.03	8.04	8.06	8.02	8.04	8.02	8.04	8.03	8.04	8.04	8.03
X_{Alm}	0.31	0.33	0.33	0.33	0.34	0.34	0.35	0.35	0.36	0.35	0.35	0.37	0.37	0.36	0.36	0.37	0.37	0.48	0.38
X_{Sps}	0.01	0.01	0.01	0.01	0.01	0.01	0.01	0.01	0.01	0.01	0.01	0.01	0.02	0.02	0.02	0.02	0.02	0.04	0.02
X_{Prp}	0.51	0.50	0.50	0.50	0.49	0.48	0.47	0.47	0.46	0.47	0.47	0.45	0.45	0.45	0.45	0.44	0.44	0.31	0.43
X_{Grs}	0.17	0.17	0.16	0.17	0.16	0.17	0.17	0.17	0.17	0.17	0.17	0.17	0.16	0.17	0.17	0.17	0.17	0.17	0.17

**Total Fe as FeO*

Sample	MT 18																		
Analysis	19	20	21	22	23	24	25	26	27	28	29	30	31	32	33	34	35	61	36
	←	←	←	←	←	←	←	←	←	←	←	←	←	←	←	←	←	Vein	←
SiO_2	39.27	39.88	39.27	39.42	39.43	39.57	39.42	39.40	39.61	39.82	39.59	39.71	39.68	39.64	39.33	39.68	39.68	38.71	39.74
TiO_2	0.00	0.01	0.00	0.01	0.00	0.02	0.01	0.00	0.00	0.00	0.00	0.00	0.00	0.02	0.00	0.00	0.02	0.03	0.03
Al_2O_3	23.00	23.40	23.19	23.16	23.02	23.13	23.22	22.84	23.14	22.96	23.09	22.99	23.16	23.35	23.16	23.19	23.16	22.43	23.09
FeO*	19.04	19.39	19.37	19.02	19.55	19.25	19.28	19.42	18.68	19.15	19.24	19.41	19.28	19.23	18.72	18.62	18.81	22.16	19.18
MnO	0.85	0.97	1.02	1.10	1.03	1.12	1.17	1.14	1.13	1.08	1.14	1.12	1.20	1.17	1.09	1.10	1.08	1.80	1.06
MgO	11.73	11.93	11.60	11.49	11.26	11.52	11.44	11.08	11.40	11.07	11.32	11.31	11.44	11.27	11.41	11.52	11.40	8.70	11.20
CaO	6.32	6.01	6.50	6.58	6.63	6.44	6.37	6.90	6.66	6.78	6.65	6.62	6.61	6.67	6.59	6.56	6.63	6.39	6.62
Total	100.21	101.59	100.95	100.78	100.92	101.05	100.91	100.78	100.62	100.86	101.03	101.16	101.37	101.35	100.30	100.67	100.78	100.22	100.92
Cations on the basis of 12 oxygens																			
Si	2.95	2.93	2.94	2.94	2.94	2.94	2.95	2.95	2.97	2.95	2.96	2.95	2.94	2.94	2.96	2.96	2.96	2.95	2.94
Ti	0.00	0.00	0.00	0.00	0.00	0.00	0.00	0.00	0.00	0.00	0.00	0.00	0.00	0.00	0.00	0.00	0.00	0.00	0.00
Al	2.04	2.04	2.04	2.03	2.03	2.04	2.02	2.03	2.02	2.03	2.02	2.03	2.04	2.04	2.04	2.03	2.03	2.04	2.03
Fe^{3+}	1.13	1.09	1.10	1.13	1.11	1.12	1.12	1.11	1.14	1.12	1.13	1.11	1.12	1.10	1.10	1.11	1.13	1.08	1.09
Fe^{2+}	0.07	0.11	0.09	0.09	0.09	0.08	0.09	0.06	0.05	0.08	0.08	0.09	0.07	0.07	0.06	0.06	0.06	0.07	0.10
Mn	0.06	0.06	0.07	0.07	0.07	0.07	0.07	0.07	0.07	0.07	0.07	0.08	0.07	0.07	0.07	0.07	0.07	0.07	0.07
Mg	1.31	1.29	1.28	1.25	1.28	1.27	1.24	1.27	1.23	1.26	1.25	1.27	1.25	1.27	1.28	1.27	1.24	1.28	1.25
Ca	0.48	0.52	0.53	0.53	0.51	0.51	0.55	0.53	0.54	0.53	0.53	0.53	0.53	0.53	0.52	0.53	0.53	0.55	0.55
Total	8.04	8.04	8.05	8.04	8.03	8.03	8.04	8.02	8.02	8.04	8.04	8.06	8.02	8.03	8.03	8.03	8.02	8.04	8.03
X_{Alm}	0.37	0.38	0.38	0.37	0.38	0.49	0.37	0.38	0.38	0.37	0.38	0.38	0.38	0.37	0.38	0.37	0.37	0.37	0.45
X_{Sps}	0.02	0.02	0.02	0.02	0.02	0.05	0.03	0.02	0.02	0.02	0.02	0.02	0.02	0.03	0.02	0.02	0.02	0.02	0.04
X_{Prp}	0.44	0.44	0.43	0.43	0.42	0.29	0.43	0.43	0.41	0.43	0.42	0.42	0.42	0.42	0.42	0.43	0.43	0.43	0.33
X_{Grs}	0.17	0.16	0.17	0.18	0.18	0.17	0.17	0.17	0.19	0.18	0.18	0.18	0.18	0.18	0.18	0.18	0.18	0.18	0.18

**Total Fe as FeO*

Sample	MT 18																		
Analysis	37	60	38	39	40	41	42	43	59	44	45	46	47	48	49	50	51	52	53
	←	Vein	←	←	←	←	←	←	Vein	←	←	←	←	←	←	←	←	←	←
SiO_2	39.54	37.74	39.23	39.62	39.14	39.59	39.31	39.52	37.95	39.48	39.41	39.51	39.53	39.44	39.40	39.57	39.52	39.53	39.60
TiO_2	0.01	0.00	0.04	0.02	0.01	0.03	0.00	0.01	0.00	0.02	0.04	0.01	0.00	0.02	0.00	0.02	0.02	0.01	0.00
Al_2O_3	23.14	21.86	23.01	22.97	22.92	23.06	23.07	23.00	21.83	23.03	22.96	23.10	23.14	22.97	22.67	23.00	23.08	22.89	22.94
FeO*	18.38	24.06	19.08	18.97	20.40	20.10	19.58	19.75	24.60	19.86	19.73	19.63	19.88	19.80	19.77	19.80	20.08	20.23	20.08
MnO	1.05	2.76	1.09	1.26	1.20	1.28	1.28	1.30	2.92	1.43	1.36	1.27	1.28	1.33	1.31	1.29	1.47	1.36	1.26
MgO	11.47	6.40	11.24	11.25	11.11	10.79	11.07	11.09	6.61	10.91	10.83	10.97	10.83	10.73	10.71	10.85	10.82	11.05	10.51
CaO	6.92	6.73	6.90	6.53	6.50	6.27	6.40	6.41	6.25	6.42	6.44	6.24	6.35	6.27	6.31	6.38	6.31	6.30	6.43
Total	100.51	99.55	100.59	100.62	101.28	101.12	100.71	101.08	100.16	101.15	100.77	100.73	101.01	100.56	100.17	100.91	101.28	101.37	100.82
Cations on the basis of 12 oxygens																			
Si	2.96	2.93	2.96	2.94	2.95	2.95	2.95	2.96	2.95	2.96	2.97	2.96	2.95	2.95	2.97	2.96	2.96	2.95	2.95
Ti	0.00	0.00	0.00	0.00	0.00	0.00	0.00	0.00	0.00	0.00	0.00	0.00	0.00	0.00	0.00	0.00	0.00	0.00	0.00
Al	2.02	2.02	2.03	2.04	2.02	2.03	2.03	2.04	2.04	2.03	2.01	2.03	2.03	2.01	2.03	2.03	2.01	2.02	2.01
Fe^{3+}	1.12	1.15	1.19	1.14	1.15	1.16	1.16	1.17	1.18	1.19	1.19	1.18	1.18	1.16	1.21	1.19	1.45	1.50	1.48
Fe^{2+}	0.06	0.13	0.06	0.08	0.08	0.08	0.07	0.06	0.06	0.05	0.06	0.06	0.08	0.10	0.05	0.06	0.08	0.08	0.09
Mn	0.08	0.08	0.08	0.08	0.08	0.09	0.09	0.08	0.08	0.08	0.08	0.08	0.09	0.09	0.08	0.08	0.15	0.16	0.18
Mg	1.25	1.24	1.20	1.24	1.23	1.21	1.21	1.22	1.21	1.20	1.20	1.21	1.20	1.23	1.17	1.19	0.88	0.80	0.87
Ca	0.52	0.52	0.50	0.51	0.51	0.51	0.52	0.50	0.51	0.50	0.51	0.51	0.50	0.50	0.52	0.51	0.50	0.52	0.46
Total	8.01	8.07	8.02	8.03	8.02	8.03	8.03	8.03	8.03	8.01	8.02	8.03	8.03	8.04	8.03	8.02	8.03	8.02	8.04
X_{Alm}	0.38	0.36	0.50	0.37	0.38	0.38	0.40	0.38	0.39	0.51	0.39	0.39	0.39	0.40	0.40	0.40	0.40	0.40	0.39
X_{Sps}	0.02	0.02	0.06	0.02	0.02	0.03	0.03	0.03	0.03	0.06	0.03	0.03	0.03	0.03	0.03	0.03	0.03	0.03	0.03
X_{Prp}	0.42	0.43	0.25	0.42	0.42	0.42	0.40	0.42	0.41	0.26	0.41	0.41	0.41	0.41	0.40	0.40	0.40	0.40	0.41
X_{Grs}	0.18	0.19	0.19	0.19	0.18	0.17	0.17	0.17	0.17	0.17	0.17	0.17	0.17	0.17	0.17	0.17	0.17	0.17	0.17

**Total Fe as FeO*

Table 1. (continued)

Sample	MT 18																		
Analysis	54	55	56	57	58	4	5	6	7	8	9	10	11	12	13	14	15	16	17
	←	Core																	
SiO_2	39.33	38.22	38.18	37.81	37.39	40.57	40.56	40.38	38.91	39.12	39.67	40.10	40.08	40.55	40.19	39.46	39.87	39.98	38.71
TiO_2	0.01	0.00	0.02	0.00	0.02	0.05	0.00	0.01	0.01	0.00	0.00	0.00	0.01	0.01	0.01	0.01	0.00	0.00	0.00
Al_2O_3	22.88	21.80	22.01	21.95	21.55	22.75	22.80	22.61	21.62	22.85	22.87	23.05	22.96	22.73	22.70	22.65	23.07	22.77	22.27
FeO*	19.85	24.60	23.71	24.13	23.70	18.17	17.93	17.49	21.86	19.02	18.24	18.71	18.33	18.00	18.55	18.09	19.31	19.17	18.82
MnO	1.20	3.35	2.22	2.43	2.73	0.37	0.35	0.36	1.36	0.54	0.43	0.46	0.51	0.43	0.46	0.48	0.58	0.57	0.54
MgO	10.64	6.25	7.62	6.91	7.40	13.61	13.68	13.49	9.65	12.60	12.95	13.10	12.96	12.81	12.75	12.49	12.46	12.36	12.24
CaO	6.36	6.26	6.05	6.25	5.42	5.98	5.98	5.91	5.46	5.83	5.72	5.69	5.61	5.65	5.60	5.75	5.96	5.75	5.75
Total	100.27	100.48	99.81	99.48	98.21	101.51	101.29	100.25	98.87	99.95	99.87	101.12	100.45	100.17	100.27	98.93	101.24	100.60	98.32
Cations on the basis of 12 oxygens																			
Si	2.95	2.95	2.95	2.94	2.94	2.96	2.96	2.98	2.99	2.91	2.95	2.94	2.96	3.01	2.98	2.96	2.94	2.96	2.93
Ti	0.00	0.00	0.00	0.00	0.00	0.00	0.00	0.00	0.00	0.00	0.00	0.00	0.00	0.00	0.00	0.00	0.00	0.00	0.00
Al	2.00	2.02	2.00	2.01	2.00	1.96	1.96	1.97	1.96	2.00	2.00	2.00	2.00	1.99	1.98	2.01	2.00	1.99	1.99
Fe^{3+}	1.51	1.49	0.10	0.11	0.12	0.12	0.11	0.07	0.06	0.17	0.10	0.12	0.07	0.00	0.05	0.06	0.13	0.08	0.14
Fe^{2+}	0.09	0.08	1.43	1.46	1.43	0.99	0.98	1.01	1.35	1.01	1.03	1.03	1.06	1.12	1.10	1.07	1.06	1.11	1.05
Mn	0.19	0.18	0.14	0.16	0.18	0.02	0.02	0.02	0.09	0.03	0.03	0.03	0.03	0.03	0.03	0.03	0.04	0.04	0.03
Mg	0.77	0.75	0.88	0.80	0.87	1.48	1.49	1.48	1.11	1.40	1.43	1.43	1.43	1.42	1.41	1.40	1.37	1.37	1.38
Ca	0.52	0.56	0.50	0.52	0.46	0.47	0.47	0.47	0.45	0.47	0.45	0.45	0.44	0.45	0.44	0.46	0.47	0.46	0.47
Total	8.03	8.03	8.00	8.00	8.00	8.00	8.00	8.00	8.00	8.00	8.00	8.00	8.00	8.00	8.00	8.00	8.00	8.00	8.00
X_{Alm}	0.41	0.40	0.48	0.50	0.49	0.33	0.33	0.34	0.45	0.35	0.35	0.35	0.36	0.37	0.37	0.36	0.36	0.37	0.36
X_{Sps}	0.03	0.03	0.05	0.05	0.06	0.01	0.01	0.01	0.03	0.01	0.01	0.01	0.01	0.01	0.01	0.01	0.01	0.01	0.01
X_{Prp}	0.39	0.40	0.30	0.27	0.30	0.50	0.50	0.50	0.37	0.48	0.49	0.49	0.48	0.47	0.47	0.47	0.47	0.46	0.47
X_{Grs}	0.17	0.17	0.17	0.18	0.15	0.16	0.16	0.15	0.15	0.06	0.15	0.15	0.15	0.15	0.15	0.16	0.16	0.16	0.16

**Total Fe as FeO*